Predictions from Macrohomogeneous Model of Aerospace Ni-Cd Battery

B. V. Ratnakumar, P. Timmerman, C. Sanchez, S. Di Stefano and G. Halpert

Jet Propulsion Laboratory, California Institute of Technology

4800 Oak Grove Dr., Pasadena, California 91109

ABSTRACT

The mathematical model developed at Texas A & M University (TAMU) for a sealed nickel - cadmium cell is modified to enable predictions of an aerospace nickel-cadmium battery under any desired charge - discharge schedule. The cell model is based on a macrohomogeneous description of porous electrodes and takes into account various processes such as mass transport in the liquid phase, charge transfer and solid-state diffusion of proton in the nickel oxide. The relevant equations for the above processes are solved by a numerical approach. In this paper, the various parameters describing the above phenomenon have been optimized to obtain a closer prediction of the charge-discharge behavior of an aerospace cell. Upon optimizing the model parameters, the performance of the aerospace nickel-cadmium cell is simulated under various experimental conditions, i.e., at different rates and temperatures. Finally, generic Ragone plots for the cell and typical Tafel plots for cadmium and nickel electrodes at various state of charge are constructed from the simulations and compared with the experimental data,

1.0 INTRODUCTION

Prediction of battery performance through simulated tests using appropriate models would provide useful guidelines for a proper management of a power subsystem on a spacecraft. JPL has been involved for the past few years in the development of mathematical models for aerospace, sealed nickel- cadmium and nickel - hydrogen rechargeable cells. These battery models have been built around the cell models developed at Texas A & M University [1-5], utilizing the macrohomogeneous (volume averaging distributed quantities such as porosity and conductivity over homogeneous mixtures of electrode and electrolyte phases) approach of Newman[6]. Various aspects addressed in the cell model include : 1) material balance for the dissolved species generated/consumed by the electrochemical reaction and transported by diffusion and migration, 2) variations in the electrode porosity due to differences in the molar volume of the reactant and products, 3) changes in the electrochemical potential in the solid phase or in the electrolyte, 4) charge transfer kinetics through a generalized Butler -, Volmer rate equation, 5) principles of conservation of charge in the electrochemical cell, and 6) effects of intercalation and slow diffision of proton into the positive electrode. The governing equations for the above phenomena are solved for each of the regions (positive electrode, separator and negative electrode) with appropriate boundary and initial conditions by the finite-differential approach using the Pentadiagonal or Tridiagonal BAND J method(7).

These models have been further modified at JPL by incorporating ohmic and semi-conductor effects at the oxide film on the positive electrode(s). The latter are introduced to explain asymmetric current-independent overpotentials observed in the positive electrode required to obtain a closer fit with cell data(9). Further improvements made at JPL in translating the basic cell model into a useful battery engineering tool include 1) a translator routine, i.e., a design input data file cent aining the electrode/cell manufacturer's details to permit simulation of any cell 2) a charge definition routine containing operational data files which allow the implementation of any discharge and/or charge protocol, and

3) incorporation of a multi-cell configuration in the battery design to model its thermal and electrical characteristics.

'l'he translator routine provides several functions to translate the cell design database containing three-dimensional parameters into the corresponding one-dimensional parameters that the model recognizes. Typical design parameters fed into the translator routine include the number of positive and negative plates, their dimensions, areas, component volumes and the porosities.

The charge definition routine defines the test conditions for the simulation, expressed as several steps of charge/discharge. Any random charge and discharge sequence can be specified. Each of these phases can accept a wide range of spacecraft charge and discharge specifications. This routine is capable of accepting five different types of control : constant current, constant voltage, constant power, constant resistance, and temperature-compensated constant potential (VT) to avoid thermal runaway during overcharge. The charge definition routine thus permits simulation under various conditions, e.g., at constant power to mimic the array output limitations, at constant current to mimic the power electronics capabilities, and at constant VT to simulate spacecraft application. In addition, a range of charge and discharge controls is available, i.e., charge or discharge can be limited by either temperature, recharge fraction, current, voltage or VT level. Though designed for the spacecraft applications, the charge definition routine is versatile and can be used in commercial applications as well.

The thermal model is implemented as a system of nodes, representing the battery and the spacecraft environment) and is solved based on finite - element approach. The nodal depiction is simplified 10 a single unit cell from a whole battery, using arguments of symmetry. The model runs concurrently with the performance model using the output from the latter, e.g., current, voltage and efficiency, to calculate the rate of heat generated. Finally, the effects of temperature on the cell properties are estimated. Thé

thermal model thus permits simulation of the cell tests under non-isothermal conditions also,' which is critical to charging in the spacecraft.

The model is thus fairly complete, and is capable of predicting the performance of any Ni-Cd cell under given test conditions, especially tests simulating the spacecraft applications. The capability of this model is demonstrated here by simulating the performance of a 50 Ah Ni-Cd cell (50AB35), manufactured by Gates Aerospace Battery Division for the TOPEX-Posiedon mission. Based on the cell qualification data on the above cell , the mode! has been calibrated with respect to several parameters pertaining to various polarization losses existing in the cell. Using the optimized values for the fundamental and design parameters, simulations have been made for the performance of the Ni-Cd cell under various experimental conditions.

2.0 POLARIZATION LOSSES

One of the deficiencies of the earlier versions of this model is an incomplete estimate of the polarization losses, as evident from capacities close to the theoretical value even at high discharge rates. The current model accounts for all possible polarizations in the Ni-Cd cell during charge as well as discharge; a) kinetic polarization related to the charge transfer across the elect rode/electrolyte interfaces, b) mass transfer polarization due to a slow diffusion of protons in the positive electrode material and c) a significant ohmic polarization electrolyte and especially across the film of active material on the positive electrode due to a large drop in the electrode conductivity at low states of charge. Each of these polarizations are treated quantitatively in the model as described below and the corresponding parameters are optimized.

Fig. 1 shows the typical contributions to the cell polarization from its individual component overpotentials at the positive electrode and at the negative electrode. Curve 1 represents the equilibrium cell voltage (OCV) and subsequent curves reflect the changes in the cell voltage as a result of charge transfer, mass transfer and ohmic polarizations at the

positive electrode and the overall polarization at the negative electrode, respectively. Such a break-up of the overpotentials would permit a battery designer / manufacturer to better understand the effect" the design parameters on the relevant polarization. It is evident from Fig. 1 that most of the cell polarization is occurring at the positive electrode, consistent with the positive-limited design of the cell. The overpotentials at the negative electrode are relatively low and constant during the entire discharge phase, as may be expected from the excess negative capacity contained in the cell. In the following sections, therefore, the polarization losses described relate only to the nickel electrode and the processes occurring there.

2.1 Kinetic Polarization

The charge transfer polarization occurring at the (positive) electrode is quantitatively described by the familiar Butler - Volmer rate equation expressed generally as[10]

$$J_j = a_j\, i_{o,j,ref} \left[\prod_1^n \left(\frac{a_{i,o}}{a_{i,ref}}\right)^{\gamma_{i,j}-1} e^{\left(\frac{\alpha_{j,f}}{RT}\eta_j\right)} - \prod_1^n \left(\frac{a_{i,o}}{a_{i,ref}}\right)^{\gamma_{i,j}-1} e^{\left(\frac{\alpha_{j,f}}{RT}\eta_j\right)} \right] \quad (1)$$

where J is the transfer current (A), a_j is the electrode surface area, $i_{o,j}$ is the exchange current density (A/cm^2), $a_{i,o}$ and $a_{i,ref}$ are the interracial and bulk concentrations of the electro-active species, $\gamma_{I,j}$ the reaction order, $\alpha_{I,j}$, the transfer coefficient and η the overpotential. The pre-exponential term in the above equation, $(a_{i,o} / a_{i,ref})$ is incorporated to recognize the fact that the mass transport processes are relatively slow. The parameters in the above equation that are characteristic of the electrode reaction include the exchange current density and transfer coefficient. The electrode area is a design-related parameter that can affect the kinetic polarization. The effects of these three parameters on the cell capacity and the cell voltages (i.e., mid-point voltages) have therefore been studied.

Fig, 2 shows the effect of the exchange cd. on the capacity and mid-point voltage of the cell. The cell capacity is fairly independent of the exchange current density, above a value of 10 $\mu A/cm^2$. Lower exchange current densities result in a decrease in the cell capacity.

The mid-point voltage levels off at an exchange cd. of 200 $\mu A/cm^2$. For the subsequent predictions, the optimum value for the exchange current density was chosen as the lowest value corresponding to minimum kinetic polarization, i.e., 200 $\mu A/cm^2$. This is within the same range as used in the earlier studies (60 $\mu A/cm^2$)[2,3].

Our simulations have shown that he area of the electrode has no noticeable effect on the cell capacity in the range of 300 to 20000 cm-l. The mid-point voltage, on the other hand, changes sharply with the area of the electrode below 5000 cm^{-1} and is insensitive after 10000 cm^{-1}. It maybe noted that the effect of the area should be the same as that of the exchange current density on the mid-point voltage, since it is their product that determines the kinetic polarization. The area of the positive electrode is thus chosen to be 10000 cm^{-1} to have minimum effect on the polarization.

Finally, the transfer coefficient for the Ni reaction at the positive electrode is expected to affect the shape of the discharge curve rather than the capacity. Fig. 3 illustrates the effect of the cathodic transfer coefficient on the discharge behavior of the positive electrode. The mid-point voltage as well as the capacity remain unaffected by a change in the transfer coefficient in the range of 0.1 to 0.9. The shape of the discharge curve, however, changes marginally; the curves, more drawn out (S shaped) at low transfer coefficients. Similar trend was observed earlier from a zero-dimensional model, in the effect of the transfer coefficient on the discharge behavioral [1].

2.2 **Polarization due to Slow Proton Diffusion**

It has been long since realized that slow difision of protons in the lattice of the positive electrode material might contribute to mass transfer polarization which in turn affects the utilization of the positive electrode at high discharge rates[12]. Reported diffusion coefficients vary from 10^{-9} to 10^{-12} cm^2/s[13-14]. A correction for the slow diffusion of the proton in the positive electrode is provided in this model by replacing the bulk concentration with the interracial proton concentration, which in turn is determined using Fick's laws of diffusion, The diffusion of the proton is viewed to occur across the layers

of the active materials inside the pores of the electrode, i.e., in a direction perpendicular to , the solution current and parallel to the electrode. Fig. 4 shows the effect of the proton diffusion coefficient on the discharge behavior of the Ni-Cd cell. There is a pronounced effect of the diffusion coefficient on the discharge behavior at low values ($<10^{-10}$ cm^2/s). At high values ($\geq 10^{-9}$ cm^2/s), on the other hand, the mass transport is rapid enough to prevent polarization resulting from proton diffusion. The diffusion coefficient is thus chosen to be of the order of 10-9 cm^2/s, which is in agreement with the values used in the earlier modeling studies(3).

2.3 **Polarization** due to Changes in Electrode Conductivity

One of the governing equations to describe the behavior of the nickel electrode is based on the application of Ohm's law in the positive electrode, which contains σ, the conductivity of the solid phase. However, it is known that the conductivity of the positive electrode is a strong function of the state of charge of the electrode; the conductivity of the reduced phase is orders of magnitude lower than the conductivity of the oxidized phase[15]. It is essential that the conductivity of the partially discharged electrode (O < state of charge < 1) be properly defined, lest the conductivity y decline be too rapid. In this model, therefore, a modified expression, similar to that used in the nickel-hydrogen model[5-15] is used to define the conductivity, i.e.,

$$\sigma = A\, e^{-B(1-\theta)^{C}} \qquad (2)$$

where A is the conductivity of the oxidized phase, θ is the state of charge, and B and C are constants characterizing the change in the conductivity of Ni electrode during discharge. In a further improvement of the model, the above expression has been utilized to describe the conductivity changes across the oxide layer, i.e., in a direction perpendicular to the electrode. The imposed overpotentials in the electrochemical rate equation (*Eqn.1*) are corrected for the ohmic drop in the positive electrode. In order to understand the effects of the constants involved in the conductivity expression (*Eqn.* 2), sensitivity analyses have been carried out on the above three parameters. These parameters have no noticeable

effect on the discharge voltages. The capacity however, changes significantly, especially with constant B (Fig. 5). There is no change in the capacity with an increase in the value of constants A and C beyond 3 and 5, respectively . The capacity increases monotonously with a decrease in the constant B and approached the experimental value at a B value of 13. The optimum values for the constants A, B and C are chosen as 3, 13 and 5 to have the simulated capacity similar to the experimental capacity. With these values the profile of the conductivity curve during a discharge of the nickel oxide electrode is shown in Fig. 6.

2.3 Reversible potential

The simulated discharge curves are in general flatter, whereas the experimental curves are more drawn out (S-shaped). This characteristic becomes more prominent in the experimental discharge curves in the course of cycling. ***One*** of the parameters in the model influencing the shape of the curves is a term called 'intercalation constant' used in the expression for the single-electrode potential of the nickel electrode This term is introduced in the expression for the equilibrium potential of the positive electrode to account for its deviations from an ideal solid solution behavior. The discharge behavior swings from a single - phase to two-phase for an intercalation constant of O and -3, receptively. The effect of the intercalation constant on the discharge behavior (Fig. 7) is similar to that reported earlier. From a comparison with the experimental discharge profiles, the appropriate value for the intercalation constant is around -1 to +1.

2.4 Comparison with the experimental data

With the discharge model parameters thus optimized, the discharge behavior of the Ni-Cd is simulated and compared with the Topex discharge curve at C/2 and 20°C (Fig.8). The simulated discharge behavior of the Ni-Cd is in agreement with the experimental discharge curve, especially with respect to the discharge capacity and mid-point voltages. There is still some divergence with respect to the shape of the curves. The experimental curves displays more curvature in the initial stages of discharge, especially after extensive charge-discharge cycling, whereas the simulations provide relatively flat discharge curves.

This may be related to a possible generation of a nickel oxyhydroxide of different phase (other than the conventional β-NiOOH) and higher reversible potential in the electrode, e.g., γ-NiOOH during extensive cycling and/or over charge.

3.0 CHARGE CHARACTERISTICS

The charge reaction of the nickel electrode is governed by the same polarization phenomena outlined for the discharge process. In other words, polarizations results from charge transfer, slow (outward) solid state diffusion of proton and low electronic conductivity of the oxide during the charge reaction as well. It is assumed here, as a first approximation, that these polarizations are symmetric during charge and discharge, i.e., the exchange current density and the proton diffusivity are the same for the charge and discharge reactions. In addition to the above parameters, the charging of the nickel electrode is strongly affected by the oxygen evolution reaction. The oxygen evolution reaction is indeed thermodynamically favorable during charge but is prominent only in the latter portions of charge due to kinetic limitations. The charge efficiency for the nickel oxide electrode is therefore determined by the kinetics of the oxygen evolution reaction, i.e., its exchange current density. The evolved oxygen diffuses onto the negative electrode in a sealed, positive-limited cell and is recombined there, causing a roll-over in the electrode potential. The inflection in the cell voltage is thus governed by the evolution of oxygen at the Ni electrode. The subsequent rollover in the cell voltage is determined by the diffusion of oxygen to the negative electrode. The diffusion of oxygen occurs both in the electrolyte and gas (void volume) phases and is described by an effective diffusion coefficient for the combined transport. In order to achieve charge efficiency comparable to the experimental values, the exchange current density for the oxygen evolution reaction on the positive electrode requires to be optimized.

Fig. 9 shows the effect of the exchange current density for the oxygen evolution reaction on the charging of the oxide electrode. The charge curves with the exchange current density for the oxygen reaction varying from 108 to 10^{-15} are illustrated here and

compared with the experimental charging curve at C/l O. At low values of the exchange cd., (cf.: curve 6) there is no leveling of the potential after the inflection (corresponding to depletion of the active material for the main reaction) due to absence of oxygen evolution. At high values of exchange c. d. (cf.: curve 1), on the other hand, oxygen evolution begins early and the positive electrode is not charged completely due to poor charge efficiency (Fig. 9b). From a comparison with the experimental data (curve 7) with respect to the onset of oxygen evolution, the optimum value for the exchange current density is chosen as 3 x 10^{-11} A/cm^2.

4.0 PERFORMANCE AT DIFFERENT RATES

With the model parameters thus optimized, the discharge behavior of the Ni-Cd cell is examined as a function of the discharge rate (Fig. 10). Fig. 10A shows the simulated discharge curves at different rates, C/50, C/20, C/IO, C/S, C/2, C and 2C. The capacity of the cell is invariant at rates lower than C/l O (Fig. 10B); at higher rates, however, a slight reduction in the capacity of the cell is observed. Using the mid-point voltages from these discharges, a Ragone plot between the specific energy and specific power is constructed for the Ni-Cd cell (Fig. 10c). The Ragone plot indicates that energy densities in the range of35 - 50 Wh/kg are realizable from a Ni-Cd cell during discharges at a specific power of 5 to 130 W/kg. The simulated Ragone plot is in good agreement with the experimental behavior of a Ni-Cd cell[9].

The charging of the Ni-Cd cell is strongly affected by the rate. Fig 11 gives the charge curves at different rates from C/3 to C/50. The charging process seems to be most efficient at C/5- C/20; at rates $\geq$ C/3, the oxygen evolution sets in early and the cell is incompletely charged.

Further, using the charge and discharge potentials at different currents, Tafel polarization curves could be generated at a given state of charge. Fig. 12A and 12B show such Tafel curves of the Ni and Cd electrodes, respectively during oxidation as well reduction. The

Tafel curves of Cd are symmetric during oxidation and reduction, consistent with our assumption. The Tafel curves of Ni oxide, however, are asymmetric. The divergence is due to the interference of oxygen evolution reaction with the oxidation of the nickel hydroxide . Also, the Tafel plots of the nickel oxide electrode indicate strong mass transfer effects, especially at high rates of discharge, being attributed to the slow diffusion of the proton in the lattice of the positive active materials. Interestingly, the mass transfer effects are more noticeable at low states of charge, possibly due to a depletion in the intercalation sites in the nickel oxyhydroxide *or* a low diffusion coefficient at low states of charge.

S.0 PERFORMANCE AT DIFFERENT TEMPERATURES

The performance of the Ni-Cd cell is known to be affected strongly with temperature. The capacity is reduced at high temperatures as well at sub-zero temperatures,. The charge process might be inefficient under some conditions, e.g., high temperature. The performance is thus dependent on the conditions of preceding charge. Alternately, the discharge process may as well be affected, e.g., at low temperatures. In order to separate these two effects, charge and discharge processes are examined independently, the latter with the same initial state of charge at all temperatures.

Fig. 13 gives the discharge behavior of the Ni-Cd cell at C/l O and at various temperatures. The capacity is reduced marginally at high temperatures, which is not related to the inefficiency in the charging process, since the discharges were simulated with the same initial state of charge. The capacity at low temperatures is expectedly lower due to the increase in all the polarizations. The capacity is reduced to 90°/0 and 80°A of the room temperature value at -20 and -30°C. From an examination of the individual contributions from the ohmic, charge transfer and mass transfer polarizations to the overpotential, it is inferred that the increased overpotentials are mostly due to a reduced conductivity in the electrolyte as well as the oxide film on the electrode at low temperatures.

Charging process at different temperatures indicates that the charging (Fig. 15 A & B) becomes more efficient at low temperature as compared to the ambient or high temperature, which is attributed to a hindered kinetics for the parasitic oxygen evolution reaction. At temperatures lower than -20°C, however, the charging process is relatively inefficient. The optimum charge temperature is thus around -10 to +- 10° C.

7.0 CONCLUSIONS

The mathematical model for a sealed nickel - cadmium rechargeable cell, developed on first principles at the Texas A & M University, has been suitably modified to predict the performance of an aerospace battery. Various fundamental parameters that are critical to the quality of the simulations are optimized by a comparison with the performance aerospace Ni-Cd cell during cell qualification tests. From the parametric optimization, suitable values for the exchange current for positive electrode reaction, proton diffusion coefficient in the nickel oxide, conductivity parameters for the positive electrode and exchange current for oxygen evolution on Ni have been identified. This optimization has significantly improved the predictability of the model. The capability of the model is further demonstrated by simulating the charge - discharge behavior of the Ni-Cd under various conditions, i.e., at different temperatures and rates. Finally, The simulated discharge data have been recast to generate Ragone plots for the Ni-Cd cell and Tafel plots for the individual electrodes.

8.0 ACKNOWLEDGMENTS

The work described here was carried out at the Jet Propulsion Laboratory, California Institute of Technology, under contract with the National Aeronautics and Space Administration and was sponsored by Code Q.

9.0 REFERENCES

1) H. Gu, T. V. Nguyen and R. E. White, J. *Electrochem. Sot.,* 134, 2953 (1987).

2) D. Fan and R. E. White, ***J.*** *Electrochem.* ***Sot.,*** 138, 17 (1991).

3) D. Fan, "Mathematical modeling of a sealed nickel - cadmium cell", Ph. D. Dissertation, Texas A&M University (1991).

4) D. Fan and R. E. White, ***J.*** *Electrochem.* ***Sot.,1*** 38, 2952(1991).

5) Z. Mao and R. E. White, *J. Electrochem.* ***Sot., 138, 3354(1991).***

6) J. Newman and W. H. Tiedeman, *AICh E* ***Journal, 21,25*** (1***975).***

7) J. Newman, ***Industrial and Engineering Chemistry Fundamentals, 367-369*** (1 ***978).***

8) P. Timmerman, *Proc. 29th* ***inter-society*** *Energy* ***Conversion*** *Engineering Conf.*, 112 ***(1994).***

9) P. Timmerman, S. Di Stefano, P. Gluck and D. Perrone, *Proc. 26th* ***Infer-society Energy Conversion Engineering*** *Conf.* ***358(1991).***

10) A. J. Bard and I... R. Faulkner "*Electrochemical Methods:* ***Fundamentals and Applications",*** John Wiley & Sons, N. Y. (1980).

11) J. Weidncr and P. Timmerman, J. ***Electrochemical Sot.,*** 141, 346 (1994).

12) D. M. MacArthur, ***J.*** *Electrochem.* ***Sot.,*** 117,422 and 729 (1970);

13) G. W. D. Briggs and P. R. Snodin, *Electrochim.* ***Acts, 27, 565 (1982).***

14) C. Zhang and S. Park, ***J.*** *Electrochem.* ***Sot., 134, 2966(1987).***

15) Z. Mao, P. De Vidts, R. E. White and J. Newman, *J. Electrochem.* ***Sot., 141, 54 (1994).***

16) R. Barnard, C. F. Randel and F. L. Tye, ***J.*** *Appl. Electrochem.*, 10, 109 (1980).

17) D, Linden ***"Handbook on Batteries and Fuel Cells",*** McGraw-Hill, N. Y. ***(1984).***

Figure Captions

Fig. 1 : Effects of various polarization losses in the Ni-Cd cell on the discharge voltage. The curves indicate the decrease in the 1) equilibrium voltage (OCV) due to overpotential contributions from the 2) charge transfer, 3) mass transfer (slow diffusion of proton), 4) ohmic (across the oxide layer) polarizations at the positive electrode and 5) overall polarization at the Cd electrode.

Fig. 2: Effect of exchange current density of the reduction of nickel oxyhydroxide on 1) the capacity and 2) mid-point voltage during simulated discharge of a Topex cell at C/2.

Fig, 3: Simulated discharge curves of a Ni-Cd cell at C/2 with different values for the cathodic transfer coefficient of the nickel electrode, i.e., 1)0.1, 2) 0.5 and 3) 0.9.

Fig. 4: Simulated discharge curves of a Topex Ni-Cd cell at C/2, with various values for the proton diffusion coefficient in the positive electrode, i.e., 1) 8.0x 10^{12}, 2) 1.0x 10]', 3) 4.0X 10^{-11}, 4) 8.0 X 10^{-11}, 5) 1.0x 10^{-10}, 6) 4.0x 10^{-10}, 7) 8.0x 10^{-10}, and 8) 8.0x 10^{-9}, cm^2/s.

Fig. 5: Simulated effect of A) conductivity constant A, B) conductivity constant B and C) conductivity constant Con the capacity of the Ni-Cd cell at C/2.

Fig. 6: Simulated variation of the conductivity of Ni electrode with the state of charge.

Fig. 7. Simulated discharge profiles of a Ni-Cd cell with different values, 1) +1, 2) O, 3) -1 and 4) -2 for the intercalation constant, A in the expression for the reversible potential of the positive electrode.

Fig. 8: Comparison of 1) simulated discharge curve with optimized model parameters, with 2) the experimental discharge curve at C/2.

Fig. 9: Comparison of simulated charge curves with different values, i.e., 1) 3.0 x 10-9, 2) 3.0 x 10^{-10}, 3) 3.0 x 10^{-11}, 4) 3.0 x 10^{-12}, 5) 3.0 x 10^{-13}, 6) 3.0 x 10^{-14}, A/cm^2 for the exchange current density for the oxygen evolution at the Ni electrode with the 7) experimental charging curve of a Ni-Cd cell at C/l 0. Fig. 12 B shows the state of charge of the positive electrode.

Fig. 10: Simulated discharge curves of Ni-Cd cell at different rates, i.e., 1) C/20, 2) C/1 O, 3) C/5, 4) C/2, 5) C and 6) 2C. Fig. B shows the capacity as a function of the discharge rate and C) shows the Ragone plot of a Ni-Cd cell.

Fig. 11 : A) Simulated charging curves of a Ni-Cd cell at different rates, i.e., 1) C/3, 2) C/5, 3) C/10 and 4) C/20.

Fig. 12: Tafel plots of A) Ni and B) Cd electrodes during a) oxidation and c) reduction at a state of charge of 1) 0.75, 2) 0.5 and 3) 0.25, derived from the simulated discharge and charge potentials at different rates.

Fig. 13: Simulated discharge curves of a Ni-Cd cell at C/1 O and at a temperature of 1) -30, 2) -20, 3) O, 4) 20 and 5) 45° C. Fig. B shows the variation of the capacity with temperature.

Fig, 14: A) Simulated charge curves of a Ni-Cd cell at C/10 and at a temperature of 1) -30, 2) -20, 3) O, 4) 20° C and 5) 45° C. Fig. B shows the state of charge of the cell after charging at C/l O and at different temperatures.

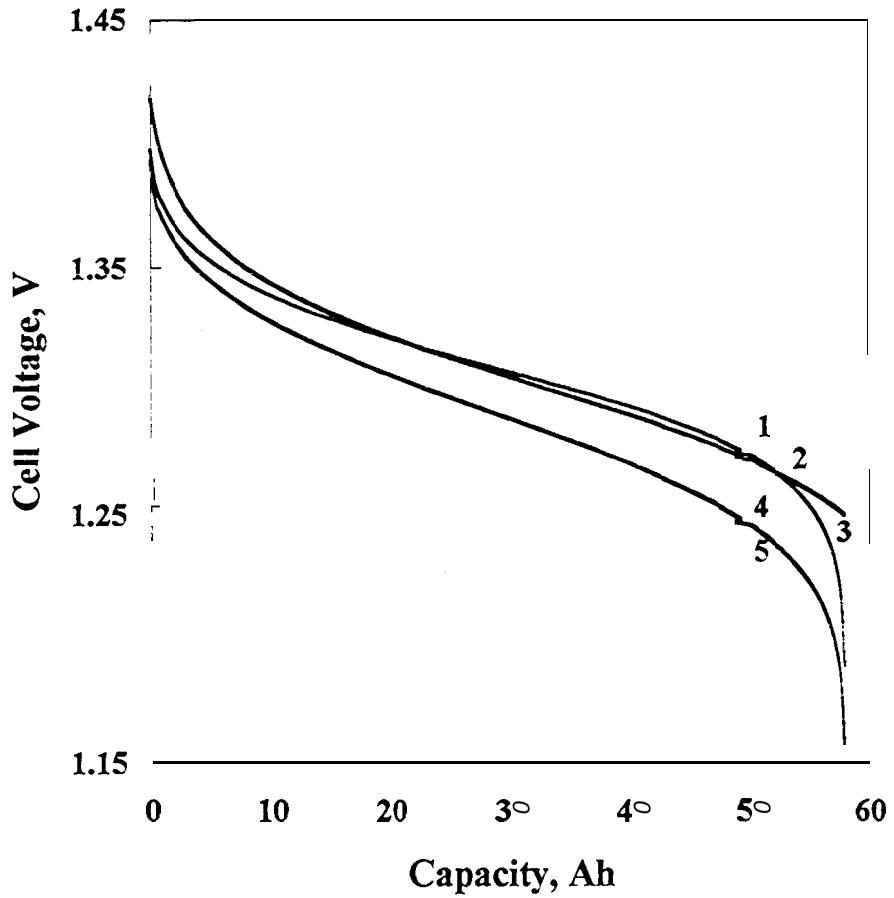
1.45
1.35
1.25
1.15
Cell Voltage, V
0
10
20
30
40
50
60
Capacity, Ah
1
2
3
4
5

Fig

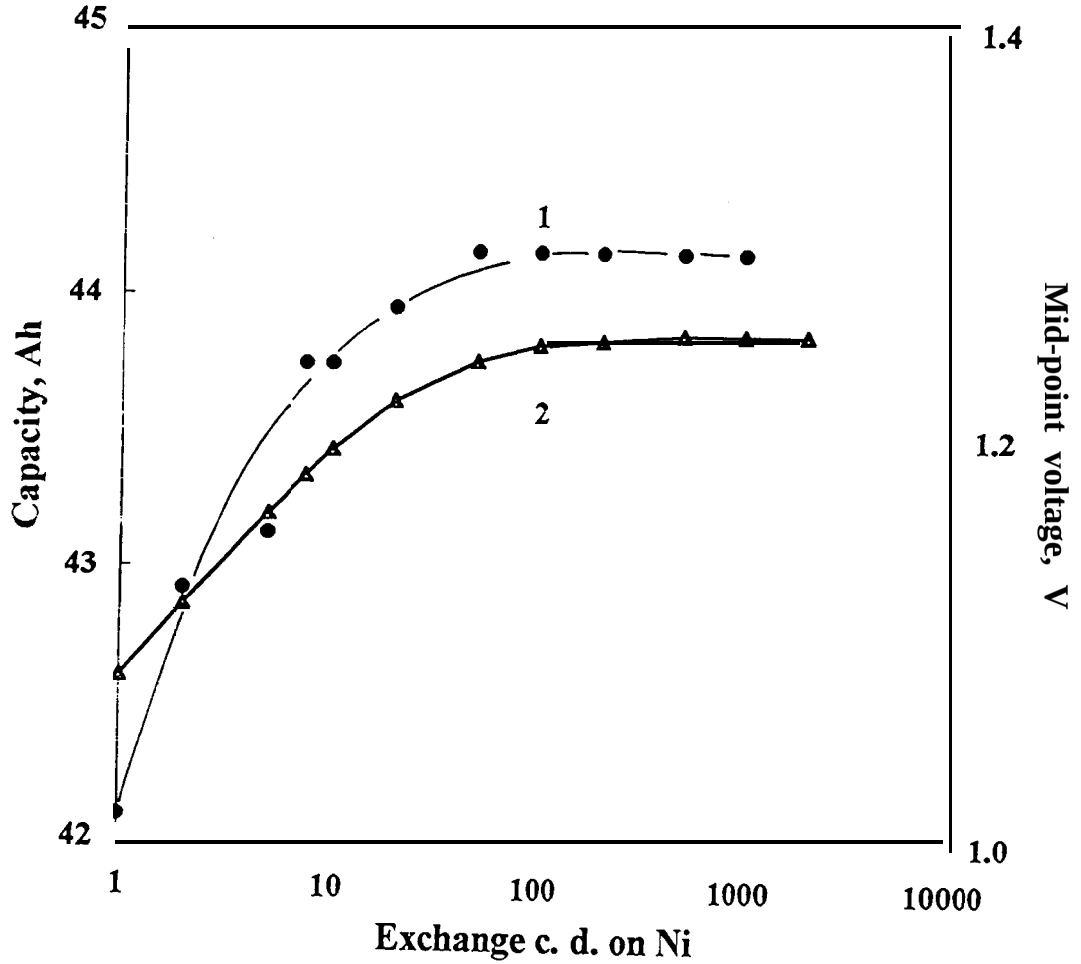
45
44
43
42
Capacity, Ah
1.4
1.2
1.0
Mid-point voltage, V
1
2
1
10
100
1000
10000
Exchange c. d. on Ni

Fig. 2

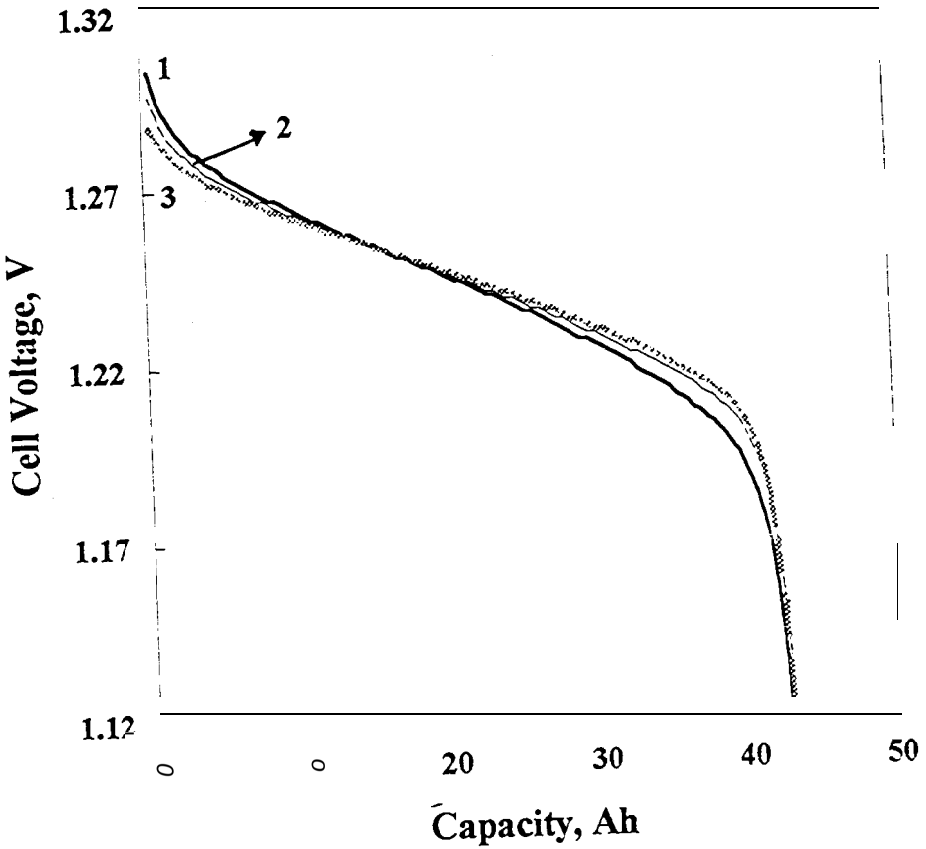
1.32
1.27
1.22
1.17
1.12
Cell Voltage, V
1
2
3
0
0
20
30
40
50
Capacity, Ah

Fig 3

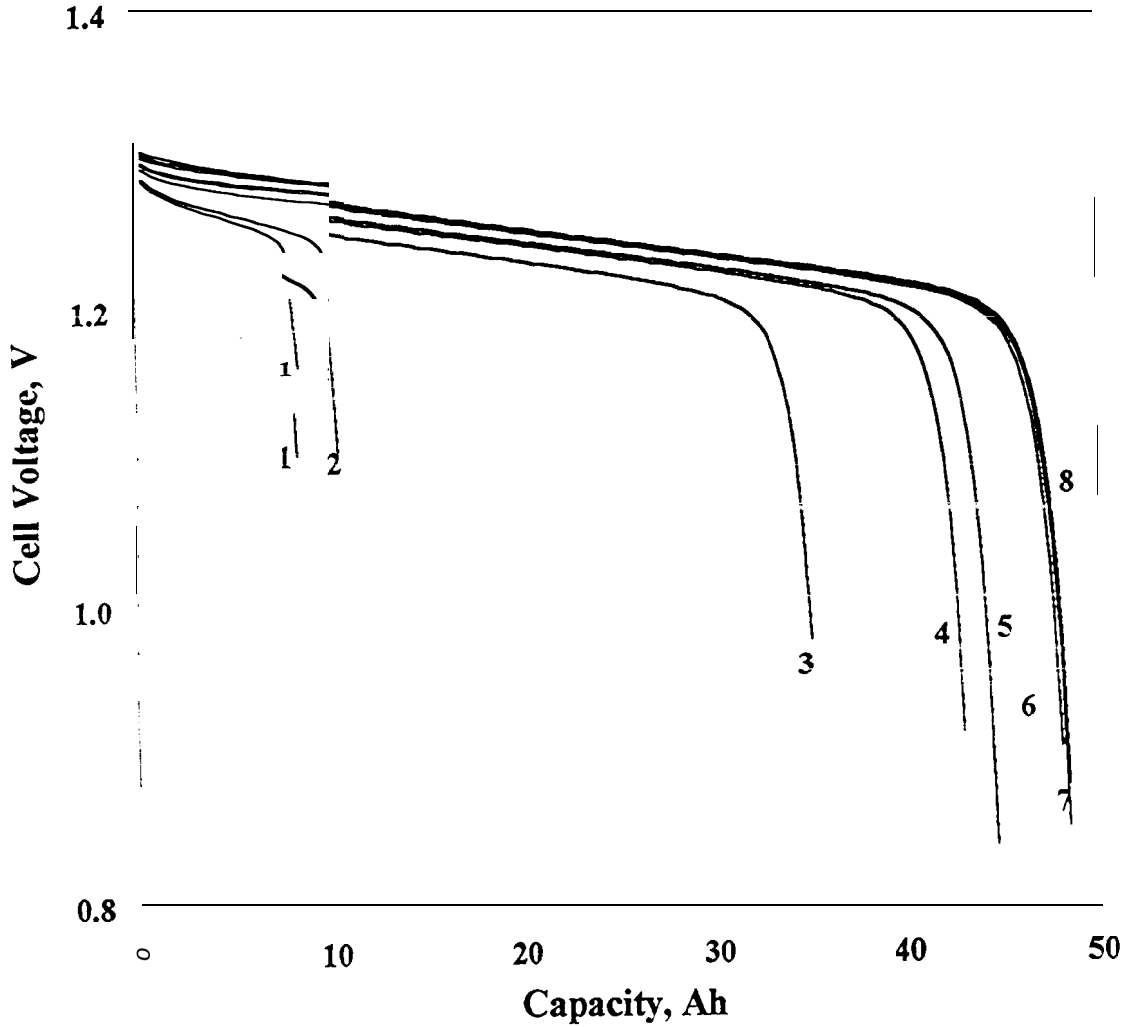
1.4
1.2
1.0
0.8
Cell Voltage, V
0
10
20
30
40
50
Capacity, Ah
1
1
2
3
4
5
6
7
8

Fg 4

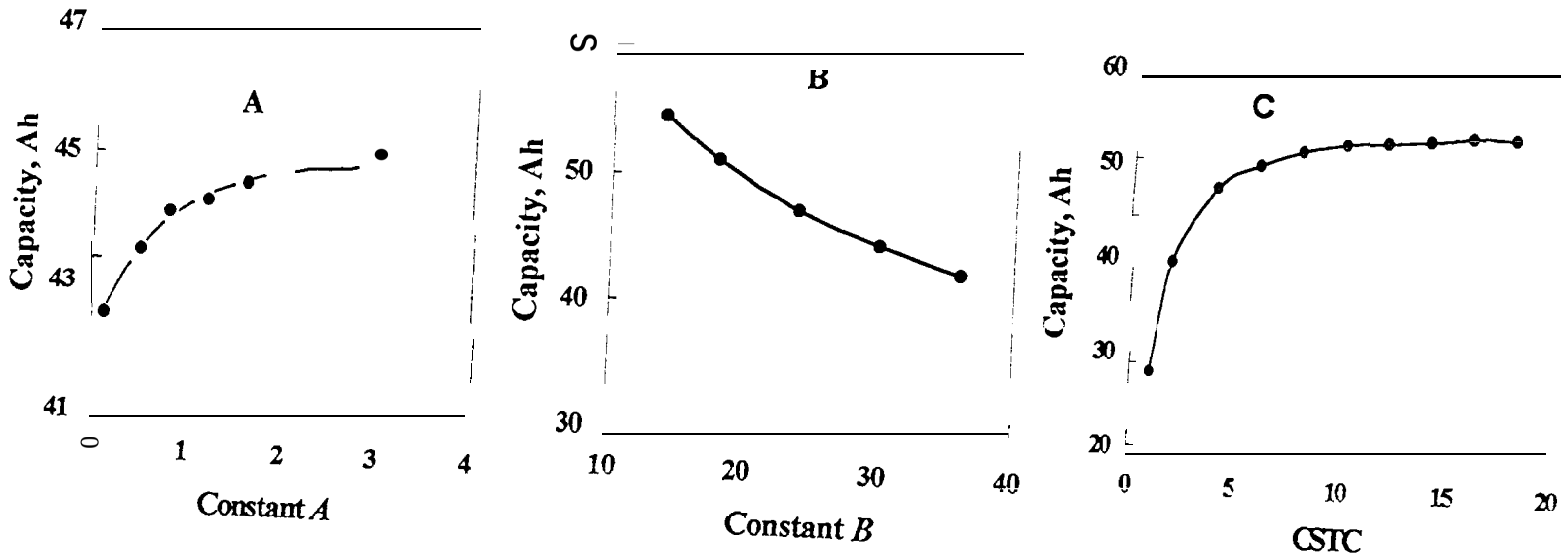
A
Capacity, Ah
47
45
43
41
0
1
2
3
4
Constant A
B
Capacity, Ah
50
40
30
10
20
30
40
Constant B
C
Capacity, Ah
60
50
40
30
20
0
5
10
15
20
CSTC

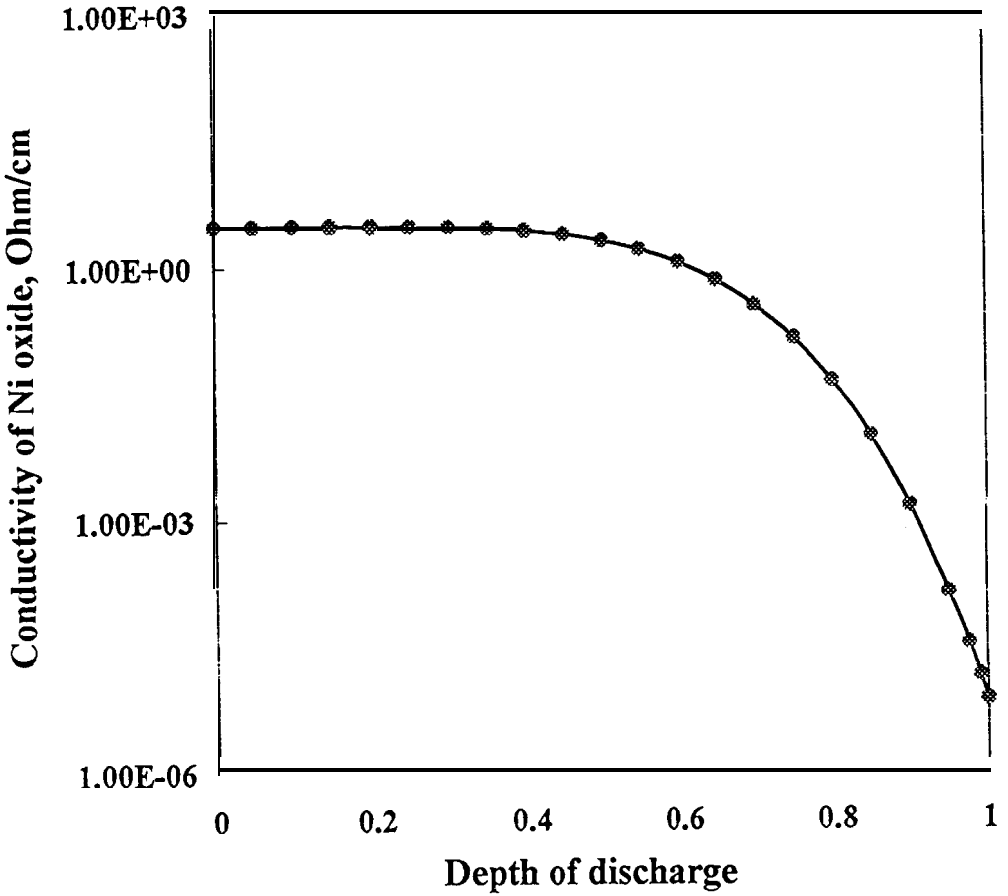
1.00E+03
1.00E+00
1.00E-03
1.00E-06
Conductivity of Ni oxide, Ohm/cm
0
0.2
0.4
0.6
0.8
1
Depth of discharge

Fig. 5

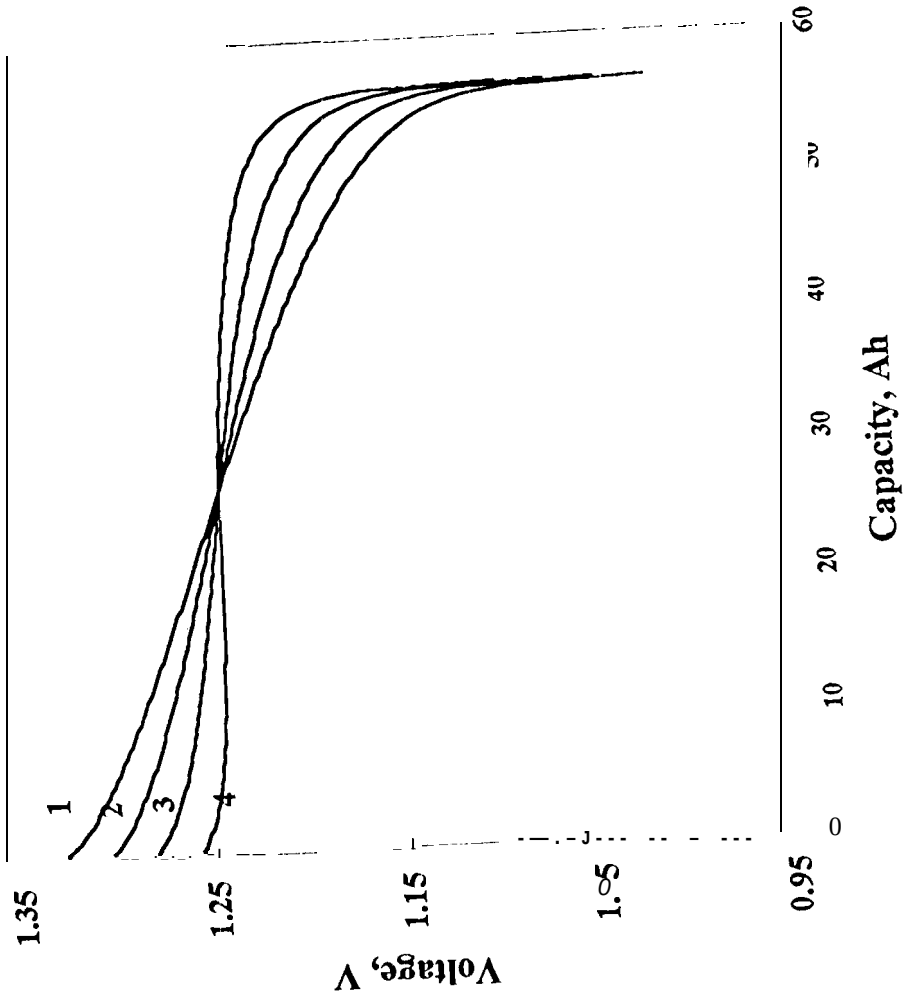
Voltage, V
1.35
1.25
1.15
1.05
0.95
Capacity, Ah
0
10
20
30
40
50
60
1
2
3
4

Fig 7

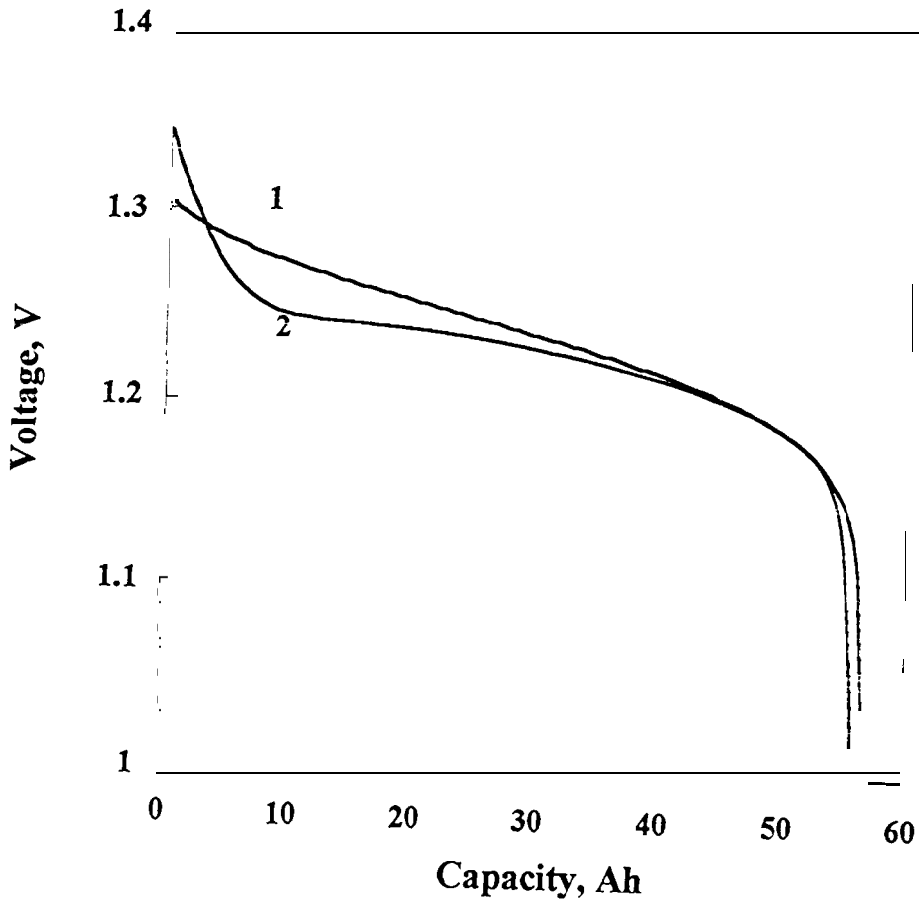

Fig. 8

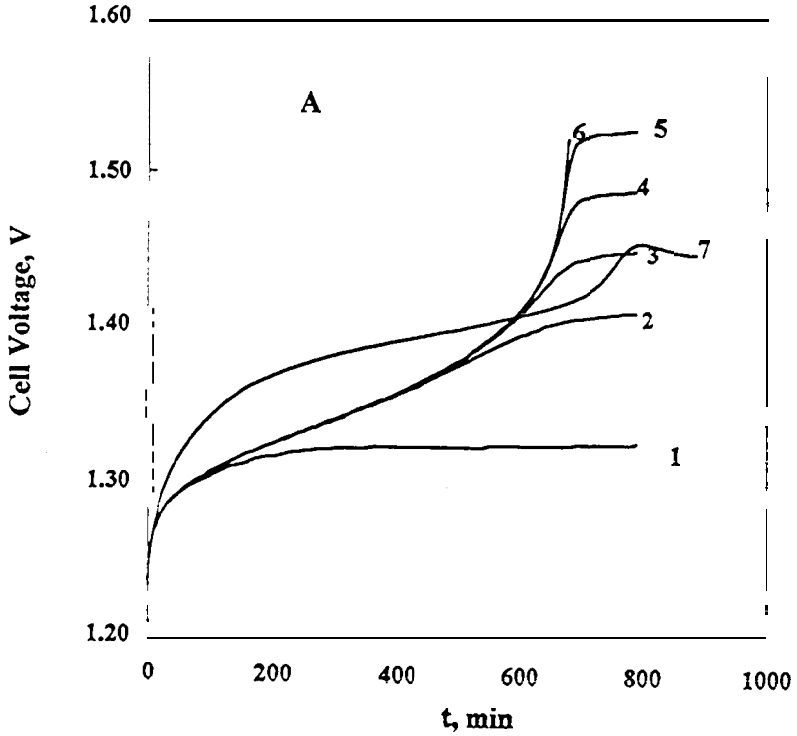
A
1.60
1.50
1.40
1.30
1.20
Cell Voltage, V
0
200
400
600
800
1000
t, min
1
2
3
4
5
6
7

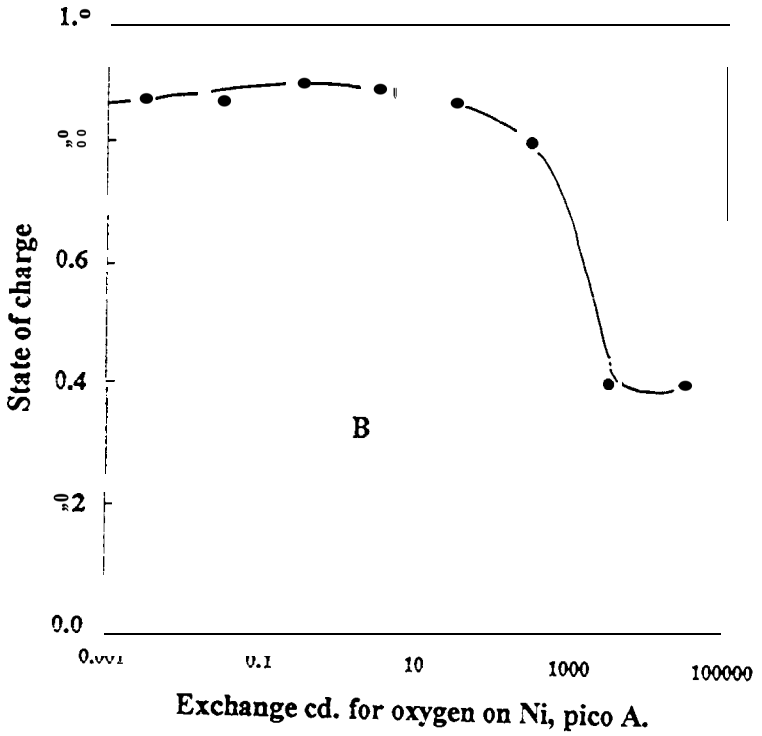
1.0
0.6
0.4
0.0
State of charge
B
0.1
10
1000
100000
Exchange cd. for oxygen on Ni, pico A.

Fig. 9

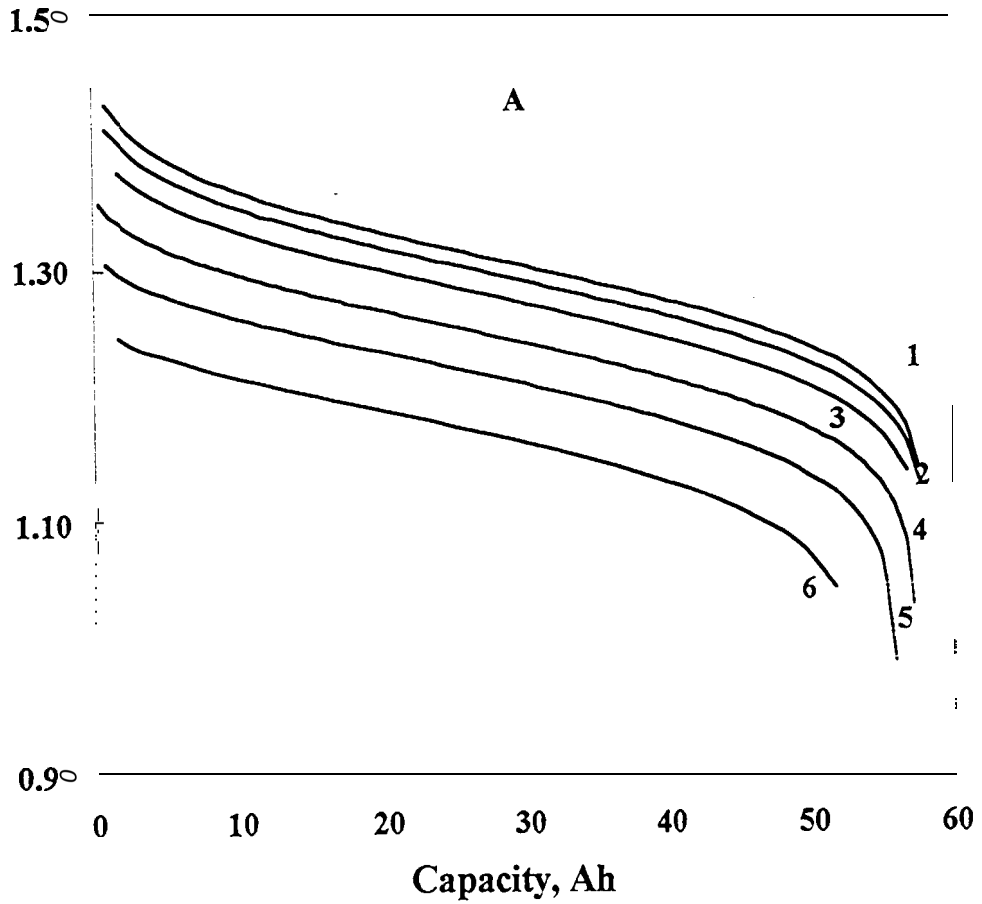

Fig 10a

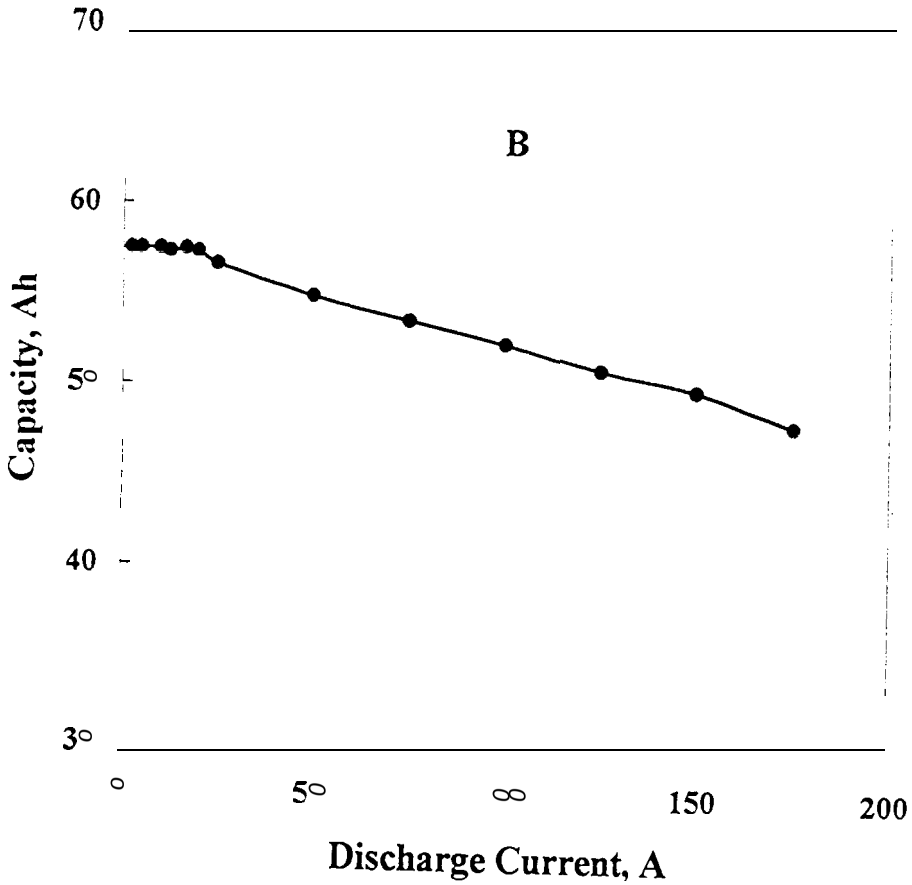

Fig. 10 B

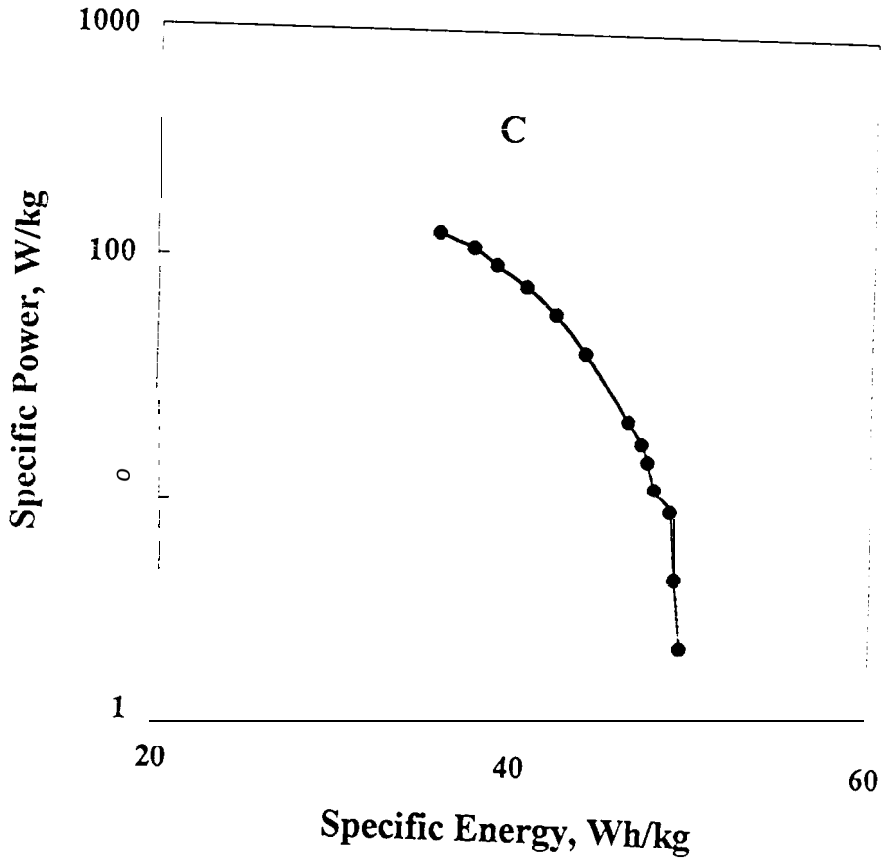

Fig 10 C

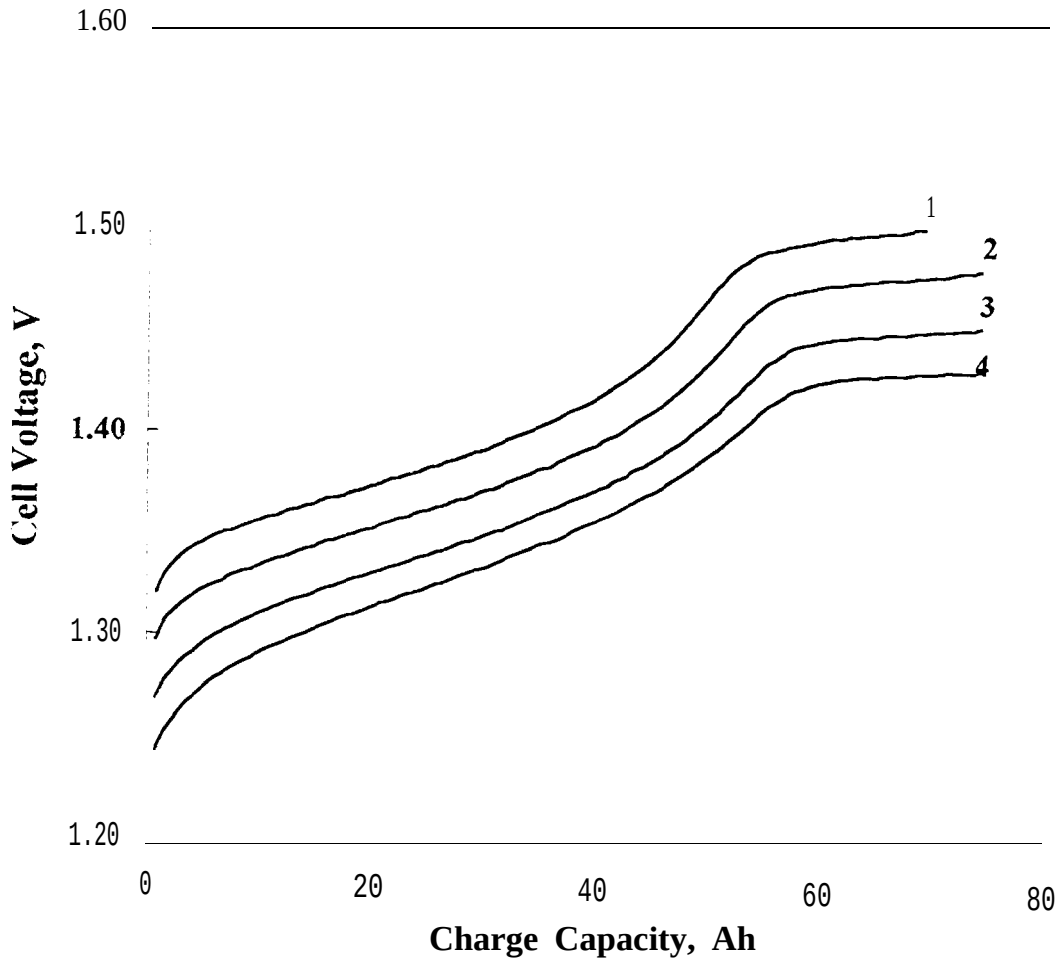
1.60
1.50
1.40
1.30
1.20
Cell Voltage, V
1
2
3
4
0
20
40
60
80
Charge Capacity, Ah

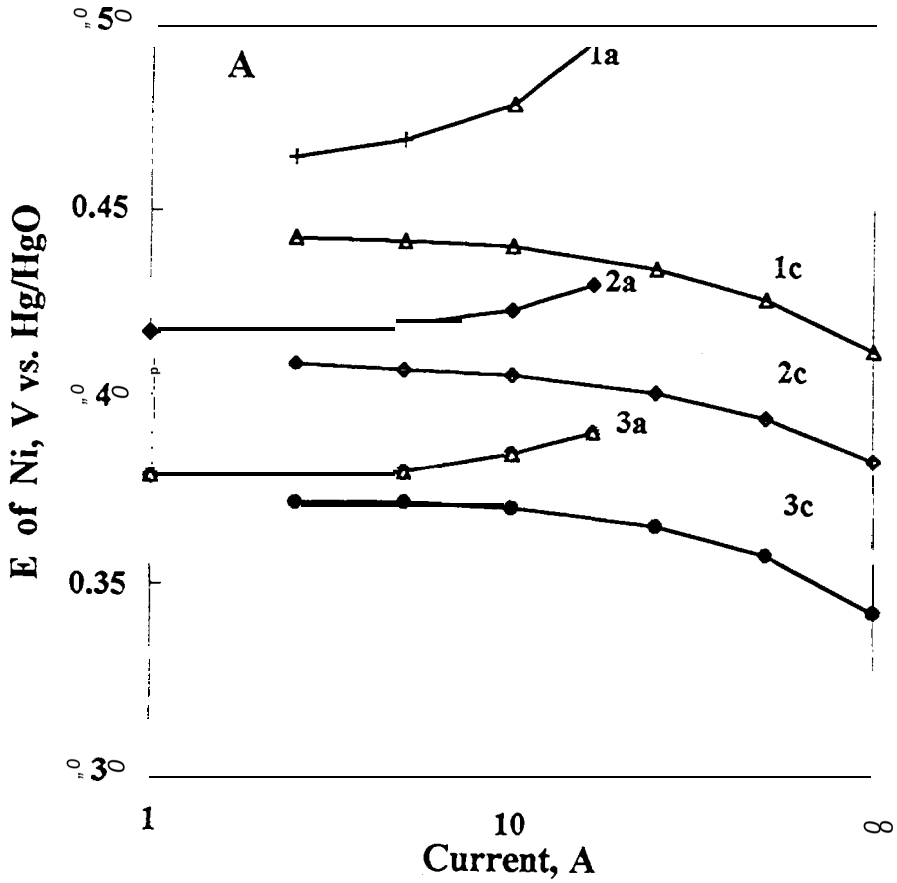
A
1a
1c
2a
2c
3a
3c
0.45
0.35
1
10
Current, A
E of Ni, V vs. Hg/HgO

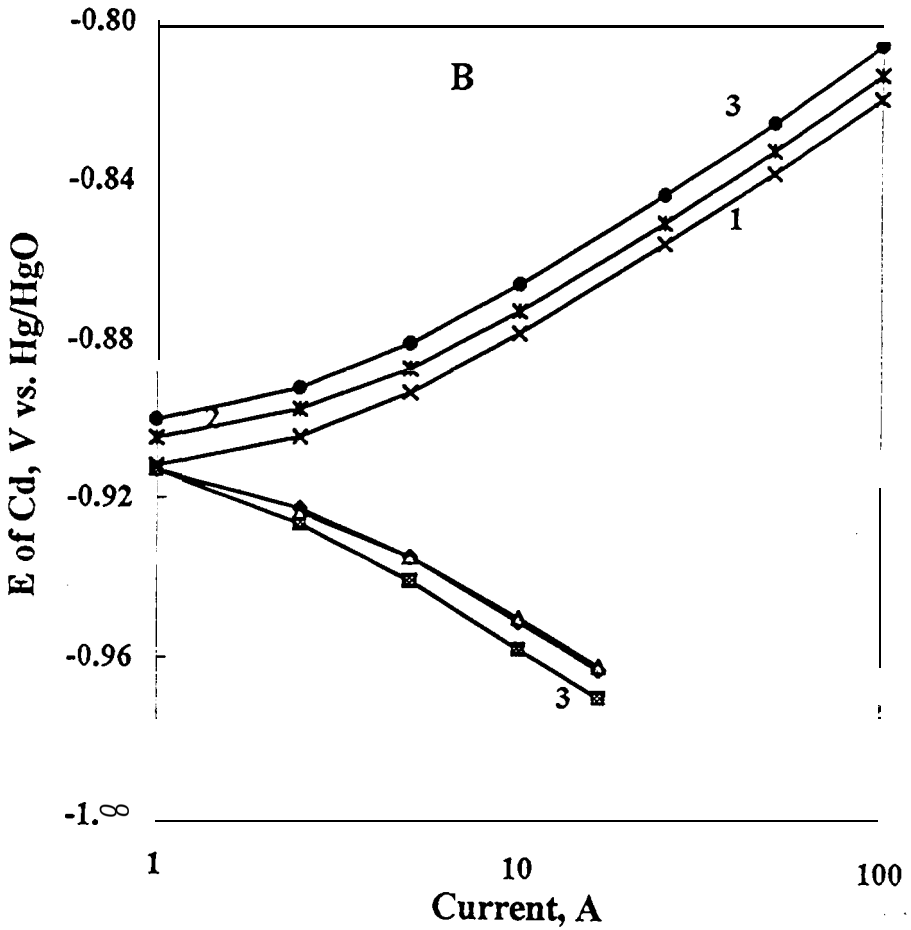
B
3
1
3
-0.80
-0.84
-0.88
-0.92
-0.96
1
10
100
Current, A
E of Cd, V vs. Hg/HgO

Fig. 12

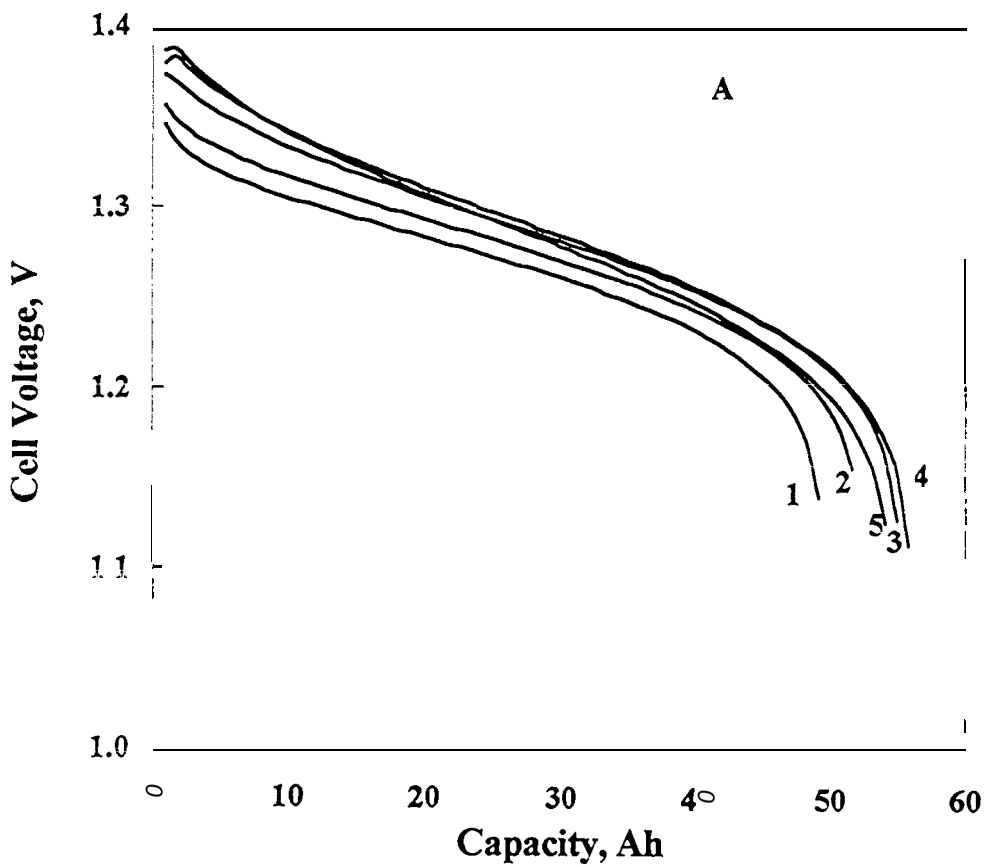
1.4
1.3
1.2
1.1
1.0
Cell Voltage, V
A
1
2
3
4
5
0
10
20
30
40
50
60
Capacity, Ah

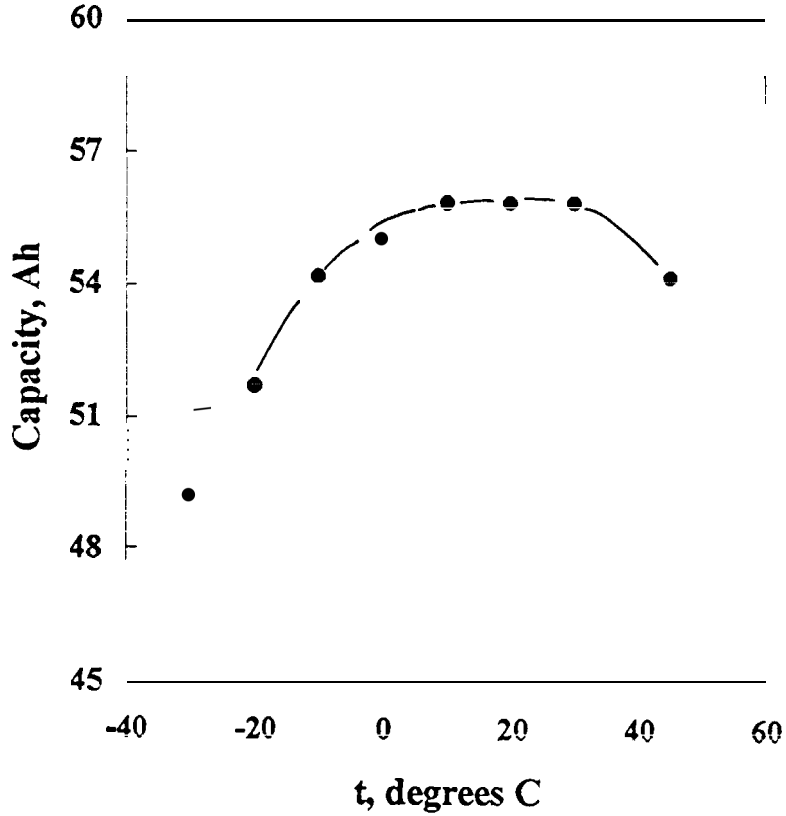
60
57
54
51
48
45
Capacity, Ah
-40
-20
0
20
40
60
t, degrees C

Fig 3

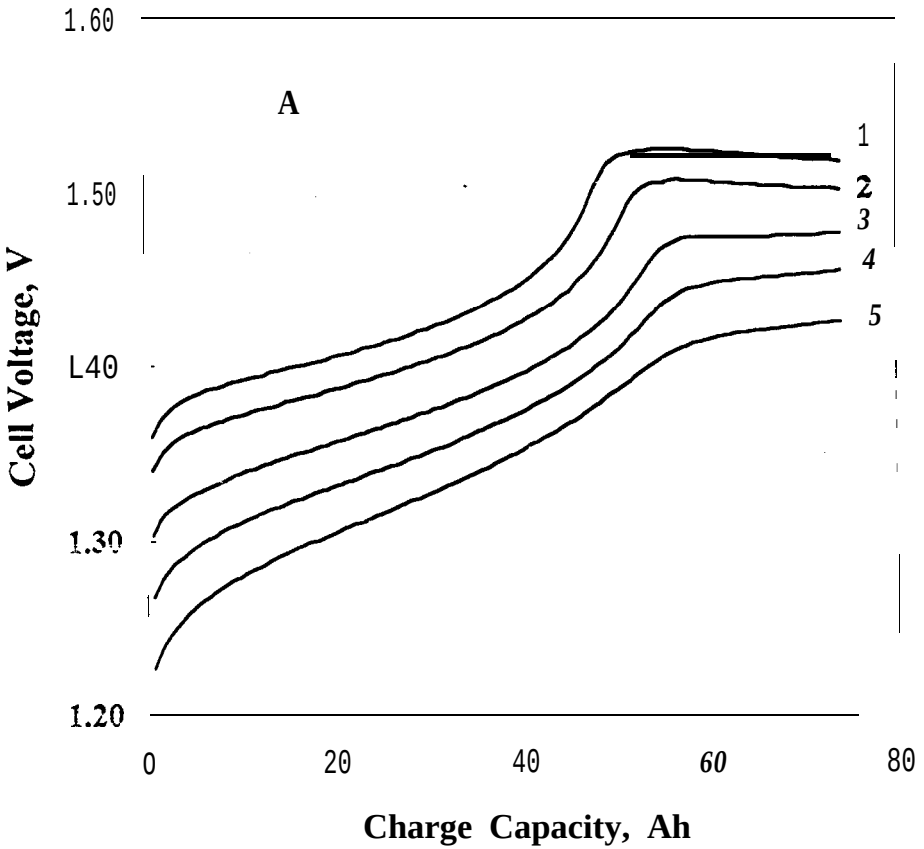
1.60
A
1.50
L40
1.30
1.20
Cell Voltage, V
1
2
3
4
5
0
20
40
60
80
Charge Capacity, Ah

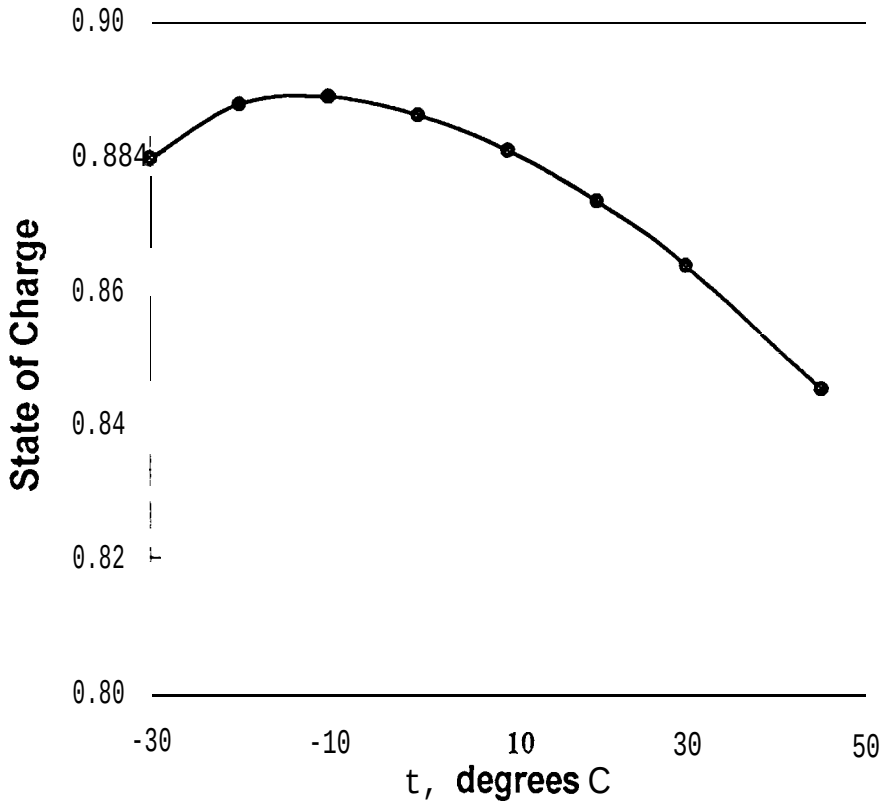
0.90
0.884
0.86
0.84
0.82
0.80
State of Charge
-30
-10
10
30
50
t, degrees C

Fig. 14